Magnetic short-range order in polycrystalline $SrGd_2O_4$ and $SrNd_2O_4$ studied by reverse Monte Carlo simulations and magnetic pair-distribution function analysis

N. Qureshi,[1,*] H. E. Fischer,[1] S. X. M. Riberolles,[1,2]
T. C. Hansen,[1] M. Ciomaga Hatnean,[2] and O. A. Petrenko[2]

[1]*Institut Laue-Langevin, 71 avenue des Martyrs, CS 20156, 38042 Grenoble Cedex 9, France*

[2]*Department of Physics, University of Warwick, Coventry CV4 7AL, United Kingdom*

(Dated: August 8, 2023)

Abstract

We present a study combining total-scattering powder neutron diffraction, reverse Monte Carlo simulations and magnetic pair-distribution function analysis to deduce both the static and dynamic short-range magnetic spin correlations in two compounds of the rare-earth strontium oxides: $SrGd_2O_4$ and $SrNd_2O_4$. Both compounds exhibit a distorted honeycomb lattice which forms a set of zig-zag ladders along the crystallographic c axis of space group $Pnam$. Each set consists of two one-dimensional chains separated by diagonal rungs forming triangles, thus inducing a large degree of geometrical frustration due to the antiferromagnetic exchange between the magnetic ions. Significant magnetic diffuse scattering was observed well above the respective Néel temperatures and analyzed with reverse Monte Carlo techniques in reciprocal space. As a complementary analysis in real space we have derived the magnetic pair-distribution function for both compounds as a function of temperature. Our results clearly indicate that the individual zig-zag ladders begin ordering well above T_N due to the dominating nearest and next-nearest interactions, long before inter-ladder spin correlations become significant only slightly above T_N. Additionally for $SrNd_2O_4$ we find some qualitative differences between the short-range spin-correlations above T_N and those observed in the ordered state.

PACS numbers:

Keywords:

I. INTRODUCTION

$SrGd_2O_4$ and $SrNd_2O_4$ belong to the large family of Lanthanide (Ln) strontium oxides, $SrLn_2O_4$, which have been extensively studied due to their rich and intriguing magnetic properties at low temperature. The groundwork was carried out by Karunadasa *et al.*[1] revealing a large variety of magnetic behaviours for different magnetic Ln ions. Later investigations by other groups reported interesting ordering phenomena including absence of long-range order in $SrDy_2O_4$ (Refs. 2–5), two coexisting types of short-range order in $SrHo_2O_4$ (Refs. 3,6,7) and a non-collinear antiferromagnetic structure in $SrYb_2O_4$ (Ref. 8). The Gd compound plays a special role among the members of this family since it reveals two magnetic phase transitions,[9,10] whereas all other members only reveal one magnetically ordered phase or none. $SrNd_2O_4$ has not received a lot of attention probably due to the more complicated synthesis route related to the high-temperature chemical instability.[11,12] The magnetic properties and the magnetic structure have recently been investigated based on powder samples.[13] While the Gd compound reveals a $k = 0$ magnetic structure with parallel nearest-neighbor spins being longitudinally ordered with respect to the one-dimensional chains along the c axis, the Nd compound has a 4 times larger magnetic unit cell described by the propagation vector $\mathbf{k} = (0\ \frac{1}{2}\ \frac{1}{2})$ and a transversal spin order with antiparallel nearest-neighbor alignment along the 1D chains.

The $SrLn_2O_4$ compounds crystallize in the orthorhombic space group *Pnam* [Fig. 1(a)] and exhibit a two-dimensional distorted Ln honeycomb lattice in the *ab*-plane [Fig. 1(b)]. Along the c axis J_1-J_2 zig-zag ladders form [Fig. 1(c)], each consisting of two 1D chains separated by diagonal rungs forming triangles that are at the heart of the geometrical frustation in this system. The nearest neighbor interactions (J_1, ~ 3.5 Å) form a one-dimensional chain along the c axis that is connected via next-nearest neighbour interactions (J_2, ~ 3.6 Å) to its partner 1D chain in a given zig-zag ladder. Inter-ladder spin separations are larger (> 3.8 Å) and play a secondary role in the magnetic exchange. The crucial detail responsible for many of the fascinating magnetic properties is the presence of two slightly different crystallographic environments for the two magnetic ions on Wyckoff site 4*c*. Nevertheless, the effect on the resulting crystal fields is huge and often leads to different easy axes or easy planes for these two sites.[3,15] An extensively studied example of this family is $SrEr_2O_4$, where the first site exhibits long-range magnetic order along a different axis compared to the second site that

exhibits only short-range magnetic order.[16,17] Furthermore, both sites reveal substantially different physics upon applying a magnetic field along the respective easy directions.[18]

Owing to the strong geometrical frustration both $SrGd_2O_4$ and $SrNd_2O_4$ display significant magnetic diffuse scattering well above the Néel temperature, but also within their magnetically ordered phases, since one of the two magnetic sites has a substantially reduced ordered moment as determined by Rietveld refinement.[10,13] We have studied the temperature dependence of the short-range spin correlations by means of total-scattering powder neutron diffraction combined with reverse Monte Carlo (RMC) simulations and magnetic pair-distribution function (mPDF) analysis, which reveal also the *dynamic* short-ranged spin correlations well above T_N and thus shed light on how the static long-range order below T_N is established in these systems as T decreases.

II. EXPERIMENTAL

The synthesis method of $SrLn_2O_4$ powders is described in Ref. 1. Quantities of $SrCO_3$ and Ln_2O_3 were finely mixed in order to obtain a chemically homogeneous mixture. In order to reduce the amount of unreacted Ln_2O_3 due to the loss of Sr through evaporation, a slightly off-stoichiometric ratio and a reaction temperature inferior to 1500°C were suggested in Ref. 9 for $SrGd_2O_4$. Therefore, an off-stoichiometric ratio of $SrCO_3$ and Gd_2O_3 (natural Gd isotope) was used corresponding to an 1:0.875 Sr excess. The mixture was pressed into pellets in order to facilitate the chemical reaction, heated to 1350°C and kept at this temperature for 48 hours. For the Nd compound the temperature should not exceed 1300°C due to the thermal stability range of the $SrNd_2O_4$ phase. An excess of $SrCO_3$ would furthermore favor chemical impurities, such as $Sr_3Nd_4O_9$ and $Sr_5Nd_8O_{17}$. Therefore, we used a stoichiometric mixture and kept it in an Al_2O_3 crucible at 1300°C for a duration of 48 hours in air. The correct phase formation was confirmed using powder X-ray diffraction, and the Rietveld refinement revealed approximately 4% of Nd_2O_3 and less than 2% of Gd_2O_3, respectively. Heat capacity and magnetization measurements (not shown) confirmed the expected magnetic transition temperatures for the $SrLn_2O_4$ phases.

Both compounds were investigated via total-scattering measurements using the hot-neutron disordered-materials diffractometer D4 (Ref. 22) at the ILL (Institut Laue Langevin, Grenoble) at a wavelength of $\lambda = 0.5$ Å that corresponds to a high incident neutron en-

ergy of 327 meV and thus a very short neutron coherence time of $\sim$ 1 fs since there is no selection/discrimination of final neutron energies reaching the detector, thus providing quasi-instantaneous *snapshots* of local atomic or magnetic structures, including therefore *dynamic* spin correlations above T_N. The powders (1.52 g of $SrNd_2O_4$ and 3.0 g of $SrGd_2O_4$, respectively) were loaded into a single-wall vanadium can that was mounted in a standard orange cryostat. Total-scattering diffraction patterns[23] were collected at various temperatures between 30 K and the base temperature 2.2 K, and a *paramagnetic baseline* pattern was recorded at 50 K, corresponding to completely uncorrelated spins in the paramagnetic state, so that it could be subtracted from the lower temperature patterns in order to remove all nuclear scattering and to retain thereby only purely magnetic scattering due to spin correlations. The CORRECT programme[24] was used for multiple-scattering and attenuation corrections as well as for normalization of the measured diffraction intensity to barns/str/atom based on the measured intensity from a vanadium standard by taking into account the sample's mass, number density and the packing fraction of its powder in the container.

In addition, in order to improve Q-space resolution as well as counting statistics vis-à-vis the relatively weak Nd magnetic moment and to check reproducibility and to compare results from two different diffractometers, the same $SrNd_2O_4$ sample was remeasured on the ILL's high-flux diffractometer D20 (Ref. 25), providing clean data[26] at 2.1 K, comfortably below $T_N \approx 2.24$ K. Other than the 2.1 K temperature point however, the data from D20 on $SrNd_2O_4$ suffered somewhat from small shifts in the positions of the very intense nuclear Bragg peaks due to sample movement (thus limiting the paramagnetic baseline temperature to only 40 K or 45 K at D20), as well as from fluctuations in the instrument background, and finally from the lack of a stable incident beam monitor. We therefore privilege the D4 data on $SrNd_2O_4$ for all temperatures except the 2.1 K data from D20.

III. RESULTS AND DISCUSSION

A. Reverse Monte Carlo simulations

The diffraction patterns in Q space have been modeled via RMC simulations using the SPINVERT program[19] after subtracting a 50 K diffraction pattern and normalizing the data

to an absolute scale as described in Sec. II. The lattice parameters for $SrGd_2O_4$ and for $SrNd_2O_4$, as well as the atomic positions of the Gd and Nd magnetic ions used in the simulations were taken from the diffraction data reported in Refs. 10 and 13, respectively. An effective local magnetic moment of $g_j\sqrt{(J(J+1)} = 7.94\ \mu_B$ and $3.62\ \mu_B$ was used for the Gd and the Nd compound, respectively. The respective magnetic form factors were described using the analytical approximation to the $\langle j_0 \rangle$ integrals for the f electrons in Gd^{3+} and Nd^{3+}.[20]

For the magnetic diffraction data on $SrGd_2O_4$ that were measured only at D4, a $9 \times 9 \times 27$ super cell (being roughly a cube of 90 Å on a side) was chosen since it is adapted to the neutron coherence volume for D4 at $\lambda = 0.5$ Å, thus matching the Q-space resolution of the simulated data with that of the experimental data. Note that SPINVERT fits in Q-space since this corresponds to the experimental measurement space. The spin dimensionality for $SrGd_2O_4$ was chosen to be Ising-like with the easy axis along c according to the reported magnetic structure at intermediate temperatures.[10] Note that the Ising model works well for several members of the $SrLn_2O_4$ family (as discussed in Ref. 27), but it would be more appropriate to describe the Gd spins with a Heisenberg model that includes significant easy-axis anisotropy, which, however, is not an option in SPINVERT (the Heisenberg model without easy-axis anisotropy fits the data in Q space equally well, but with longer simulation times). All presented calculated curves result from an average over 10 optimized spin configurations within the super cell.

For the magnetic diffraction data on $SrNd_2O_4$, the D4 data were of high quality but with limited counting statistics, whereas the D20 data had better counting statistics but were subject to some systematic errors described in Sec. II. Furthermore, other than the 2.2 K data from D4 showing unsaturated magnetic Bragg peaks, and the 2.1 K data from D20 showing well-developed sharp magnetic Bragg peaks, the diffuse magnetic scattering intensities from both instruments for $SrNd_2O_4$ at $T > T_N$ were not at all limited by instrumental Q-resolution. Therefore, in order to prevent over-fitting of random and systematic noise in the $T > T_N$ data by the SPINVERT simulations, a series of test simulations were performed with progressively smaller super cell sizes, thereby reducing the Q-space resolution of the simulations, but assuring that the super cell size was however sufficiently large to encompass the observed magnetic correlation length at each T above T_N. As a result, for $SrNd_2O_4$, SPINVERT super cells where chosen as roughly cubic with dimensions of approximately: 180 Å

(2.1 K at D20, Q-resolution-limited), 90 Å (2.2 K at D4, Q-resolution-limited), 30 Å (4.1 K, both D4 and D20), 20 Å (10 K, both D4 and D20, and 20 K for D4). Since the smaller super cells result in poorer statistics in the simulation data, an increasing number of optimized spin configurations were averaged together for progressively smaller super cell sizes. The spin dimensionality for $SrNd_2O_4$ was chosen to be easy-plane within the ab-plane following the results concerning the canted magnetic structure.[13]

In agreement with the subtraction of a 50 K paramagnetic diffraction pattern from the experimental data sets, thus retaining only magnetic scattering from spin correlations, the corresponding magnetic scattering intensities, normalized to barns/str/Ln-atom as a differential scattering cross-section, are calculated by SPINVERT according to:

$$I_{\mathrm{m}}(Q) = C[\mu f(Q)]^2 \cdot \frac{1}{N} \sum_{i \neq j} \left[A_{ij} \frac{\sin Qr_{ij}}{Qr_{ij}} + B_{ij} \left(\frac{\sin Qr_{ij}}{(Qr_{ij})^2} - \frac{\cos Qr_{ij}}{(Qr_{ij})^2} \right) \right], \qquad (1)$$

where $C = \left(\frac{\gamma_n r_e}{2}\right)^2 = p^2 = 0.07265$ barns, μ is the effective local magnetic moment in units of Bohr magnetons μ_{B}, $f(Q)$ is the magnetic form factor, N is the number of atoms in the super cell, Q is the scattering vector and the sum runs over pairs of distinct spins $i \neq j$ separated by the distance r_{ij}. In order to calculate the powder-averaged magnetic neutron diffraction intensity for each spin pair in the sum, a local coordination system is defined where z is along the vector r_{ij}, y is parallel to $\mathbf{S}_i \times \mathbf{z}$ and x completes the right-handed system. With this definition, the orientational correlation functions $A_{ij} = S_i^x S_j^x$ and $B_{ij} = 2S_i^z S_j^z - S_i^x S_j^x$ as implemented in SPINVERT.[19]

Fig. 2 shows the corrected data in absolute units for the Gd and Nd compounds together with the results of the RMC simulations. The resulting spin configurations describe all observed features very well, both the diffuse magnetic scattering (short-range spin correlations) and the magnetic Bragg peaks (long-range spin correlations). As T descends below 20 K, a diffuse magnetic scattering bump develops for both compounds at $Q \approx 1$ Å^{-1} around 10 K. This broad peak finally transforms into sharp Bragg reflections between 3.2 K and 2.4 K for the Gd compound ($T_{\mathrm{N}} \approx 2.73$ K), and between 2.2 K (D4 data) and 2.1 K (D20 data) for the Nd compound ($T_{\mathrm{N}} \approx 2.24$ K). Note that there exists an experimental uncertainty of a few tenths of degrees in the thermometry, as well as the possibility of a comparably small temperature gradient across the height of the sample, such that the 2.2 K data from D4 on the Nd compound could possibly straddle T_{N}. By comparison with the published diffraction patterns and magnetic structures,[10,13] we can attribute the strongest scattered intensities to

the magnetic (120) and (1 $\frac{1}{2}$ $\frac{1}{2}$) reflections for the Gd and the Nd compound, respectively.

The program SPINCORREL included in the SPINVERT package can be used to obtain a better understanding from a disordered system in terms of local spin correlations in real space by reducing the spin configuration in the large simulation box to the expectation value of dot products between spin-spin pairs as a function of distance, which is given by the spin-correlation function (SCF) $\langle \mathbf{S}(0) \cdot \mathbf{S}(r) \rangle$. Here, it was used to derive the SCF for all interatomic distances (shown up to 7.5 Å for selected temperatures in Fig. 3 and in Tab. I). For $T < T_N$ in the Gd compound, the positive $\langle \mathbf{S}(0) \cdot \mathbf{S}(r) \rangle$ value for the nearest-neighbour distance correctly reveals the longitudinal ferromagnetic alignment of the spins along the 1D chains parallel to the c axis [Fig. 4(a) and (b)]. This value is negative for $T < T_N$ in the Nd compound in agreement with the results from the Rietveld analysis indicating a transverse antiferromagnetic alignment of Nd spins along the 1D-chains [Fig. 4(c) and (d)]. Again for $T < T_N$, the two slightly larger distances related to Ln1-Ln1 and Ln2-Ln2 separations are significantly negative in the case of the longitudinal Gd spin alignment with respect to the chain direction which correctly accounts for the fact that two next-nearest-neighbours on the adjacent 1D chain are antiparallel [see Fig. 4(b)]. Nevertheless, due to the transversal spin alignment along the 1D chains in the Nd compound, each spin has one parallel and one antiparallel next-nearest neighbor at equal distance, which is the reason for the small value $\langle \mathbf{S}(0) \cdot \mathbf{S}(r) \rangle$ at the corresponding distances. All values of the spin-correlation function at inter-ladder distances around 4 Å, 6 Å and 7 Å are in agreement with the published models.[10,13]

For the Gd compound, we see that the static spin correlations in the long-range ordered state below T_N are qualitatively the same as the short-range dynamic spin correlations above T_N and that the latter correlations are significant.

For the Nd compound however, the situation is more complex, presumably due to the lower degree of magnetic ordering even well below T_N, amounting to only about a $^2/_3$ ordered moment for the Nd1 sites and a 10% ordered moment for the Nd2 sites.[13] We see as expected for the 2.1 K data, comfortably below $T_N \approx 2.24$ K, that the 1st distance (NN intra-chain, both Nd1 and Nd2 sites) shows AF ordering, whereas the 2nd (inter-chain/intra-ladder Nd1), 3rd (inter-chain/intra-ladder Nd2), and 4th (inter-ladder Nd1-Nd2) distances show near zero correlations, confirming among other things that there is little correlation between the spin orderings in neighboring ladders. The spin-correlations at 4.1 K for $SrNd_2O_4$ (from both

D4 and D20) show however qualitatively opposing behavior to the 2.1 K spin-correlations, namely near-zero spin correlations at the 1st distance, but AF correlations at the 2nd, 3rd (strongest), and 4th distances. Recalling that spin correlations above T_N should be dynamic and not static, we can speculate that there could be free-energy-favorable, short-ranged, short-lived (*i.e.* metastable) spin-configurations that form above T_N, but which transform to the long-range static correlations below T_N. As the 3rd distance corresponds to the inter-chain/intra-ladder for the less-ordered Nd2 sites, it is intuitive that those spin pairs have more freedom to assume (weak) AF correlations above T_N. Similar behavior is seen yet at 10 K for $SrNd_2O_4$, where as mentioned before, we favor the results from the higher-quality D4 data. The 2.2 K data from D4 show a mix of both behaviors, resulting perhaps from a sample temperature range that straddles T_N.

In order to shed light on the ordering mechanisms we focus on the correlations for selected inter-spin distances as a function of temperature, which are shown in Fig. 5. For the Gd compound, the RMC results suggest a well-defined short-range order within individual zig-zag ladders as evidenced by the non-zero SCF for nearest neighbors and next-nearest neighbors as temperature descends below $T \geq 20$ K [(green) and (blue) dots in Fig. 5 (a)]. Significant inter-ladder short-range order starts to develop later at approximately 6 K [(red) and (gray) squares in Fig. 5 (a)]. All correlations diverge at T_N marked by a vertical dashed line.

The situation is similar but more complex in $SrNd_2O_4$ [Fig. 5(b)], where for simplicity results from only D4 are shown, except for the 2.1 K points from D20. We see as expected when cooling from 10 K that the spin correlations for the intra-chain NN (3.563 Å) and intra-chain NNN (7.127 Å) distances become progressively more AF and F, respectively, but that the inter-chain/intra-ladder correlations (3.629 Å and 3.725 Å), as well as the Nd1-Nd2 inter-ladder correlations at 3.866 Å, all make an excursion to maximal AF correlations at 4.1 K before returning to near-zero correlations at 2.1 K, again suggesting the presence of short-lived/metastable short-range magnetic spin configurations. Furthermore, it is surprising that the low-temperature NNN F-correlations at 7.127 Å (twice the lattice constant c) are about a factor of two stronger than the NN AF-correlations at 3.563 Å (equivalent to the lattice constant c). Since both correlations are intra-chain this suggests that there exist above and especially below T_N within some of the nominally AF 1D chains a good number of F-ordered domains of length greater than 3 spins. Note that the comparably strong ferromagnetic

correlation at $r = 7.075$ Å refers to inter-ladder coupling of the same site (see Tab. I) and therefore mimics the behavior at the intra-chain distance. These ferromagnetic domain boundaries along the 1D chains consequently lead to weaker NN correlations in comparison to the inter-ladder correlations around 6 Å. Nevertheless, we cannot deduce directly from the SCFs whether such F-correlations are configured as longitudinal or as transverse.

B. Magnetic PDF-analysis

Although the spin-correlation functions (SCFs) discussed in the previous section have the advantage of being site-specific, their determination relies on the quality of the RMC simulations, making them somewhat model-dependent, and the simple scalar dot-product $\langle \mathbf{S}(0) \cdot \mathbf{S}(r) \rangle$ of two spins does not retain any information about the orientation of the inter-spin vector relative to the spin orientations. As such, the SCF cannot directly distinguish between e.g. longitudinal and transverse spin alignments.

Alternatively, one can retain all information in the total magnetic scattering data by performing directly a Fourier transform of the diffraction intensity once all instrument-background, multiple-scattering and attentuation corrections have been made, thus obtaining a magnetic Pair-Distribution Function (mPDF) as a function of inter-spin distance. As for atomic PDF-analysis, the mPDF(r) function represents an ensemble average of quasi-instantaneous local spin configurations, be they corresponding to static or to dynamic spin correlations.

The analytical form of mPDF(r) was derived for the first time in Ref. 21 by calculating the Fourier transform of the neutron differential scattering cross-section from a collection of magnetic moments as given in Eq. 1:

$$\begin{aligned} \mathrm{mPDF}(r) \overset{\mathrm{def}}{=} \frac{2}{\pi} \int_0^\infty Q \, \frac{I_\mathrm{m}(Q)}{\frac{2}{3}p^2\mu^2} \sin(Qr) \, dQ \\ \approx \frac{3}{2} \cdot \frac{1}{N} \sum_{i \neq j} \left[\frac{A_{ij}}{r} \tilde{\delta}(r - r_{ij}) + B_{ij} \frac{r}{r_{ij}^3} [1 - \tilde{\Theta}(r - r_{ij})] \right], \end{aligned} \quad (2)$$

where μ is the local atomic magnetic moment in units of Bohr magnetons μ_B, and $p = \gamma_n r_e/2 = 2.696$ fm as before. Note that here again we have already subtracted away the magnetic self-scattering corresponding to completely uncorrelated spins, in the same way

that a paramagnetic baseline at 50 K was subtracted from the diffraction data, in order to obtain a mPDF(r) representing only the orientational correlations between spins. Furthermore, in order to allow the comparison with the Fourier transform of the corrected $I_{\mathrm{m}}(Q)$ data, we have chosen not to divide the integrand by the magnetic form factor squared, since such a demodulation in Q-space would be tantamount to an r-space deconvolution of mPDF(r) that would be unstable numerically and would also assume a non-realistic isotropic distribution of magnetization density around the Gd and Nd ions. The mPDF(r) as calculated above therefore retains the real spatial distribution of magnetization density, and correspondingly we have replaced the delta function $\delta(r)$ and the Heaviside step function $\Theta(r)$ by Gaussian $\tilde{\delta}(r)$ and Error $\tilde{\Theta}(r)$ functions, respectively, having a full width at half maximum (FWHM) in real-space corresponding to the Fourier transform of a Gaussian fit to the squared magnetic form factor in Q-space, in accordance with the Convolution Theorem, such that: $[\mathrm{FWHM_r} = 4\ln(4)/(\mathrm{FWHM}_{f^2(Q)})]$, where $4\ln(4) \approx 5.55$ follows from the ratio of standard deviation to FWHM for a Gaussian (note that the Gaussian fit is the reason for the approximation symbol used in Eq. 2). We could therefore use the optimized spin configurations in the chosen super cell resulting from the RMC simulations to calculate directly the mPDF(r) (using the spin-correlation tool in MAG2POL[14]) and to compare it with the Fourier transformed Q-space data and fits. All Fourier transforms have been carried out with a Q_{max} of 7 Å^{-1}, as we did not observe any significant experimental magnetic intensities above that value due to the magnetic form factor approaching zero.

The results shown in Fig. 6 clearly indicate that the Gaussian approximation of the squared magnetic form factor works reasonably well since the calculated mPDF(r) [(green) dashed line] is almost identical to the Fourier transform of the RMC fit to the Q-space data [(red) dotted line]. This proves the validity of Eq. 2 and its applicability to super-cell spin-configurations as obtained from RMC simulations. The calculated mPDF(r) excellently describes the Fourier transformed data of $SrGd_2O_4$ [Fig. 6(a)] which essentially delivers the same information, but in a much more intuitive way. The generally small but visible discrepancies between the blue, red and green curves of Fig. 6(b) and (c) for $SrNd_2O_4$ are due principally to low-counting statistics (blue curve), Fourier truncation at $Q_{\mathrm{max}} = 7$ Å^{-1} (blue and red curves), and the Gaussian fit to Nd's magnetic form factor (green curve).

As mentioned earlier, the spin-correlation functions, as simple scalar dot-products of neighboring spins, cannot distinguish between longitudinal and transverse spin alignments.

For the mPDF(r) function however, as described in Ref. 21, the large negative peaks seen slightly below $r = 4$ Å in Fig. 6 stem from an antiferromagnetic alignment of two spins being separated by an inter-spin vector predominantly perpendicular to the ordered moment directions, *i.e.* a transverse AF alignment. In the case of the Gd compound this corresponds to the NNN AF correlations between two antiparallel, longitudinal F-ordered 1D chains of the same site, *i.e.* within the same zig-zag ladder. By contrast, for $SrNd_2O_4$ this strong negative peak in the mPDF(r) results from the NN transverse AF correlations between two spins of the same site on the same 1D chain, which can easily be confirmed by comparing with Figs. 4(b) and (d). For the Gd compound, the positive amplitude in the mPDF(r) between 6 and 7 Å suggests that most of the inter-chain spin correlations at those distances are transverse ferromagnetically aligned, whereas for the Nd compound, the sharper positive peak at 7 Å results principally from the NNN intra-chain spin correlations that are transverse F-aligned since corresponding to twice the NN transverse AF-aligned distance. Finally, note that the positive slope of the mPDF(r) at small r values in Fig. 6(a) is indicative of the NN longitudinal ferromagnetic order in the $SrGd_2O_4$ 1D-chains (where the point of inflection occurs at the NN distance), while the less pronounced but still positive slope in Fig. 6(b) is in agreement with the NN transverse antiferromagnetic order in the $SrNd_2O_4$ 1D-chains (where the strong negative peak occurs at the NN distance as described just above).

The most pronounced difference between the mPDFs of the two systems can be seen at $r \approx 6$ Å where the Gd compound exhibits a clear positive peak that is by contrast negative in $SrNd_2O_4$. This can again be simply explained by the different types of magnetic structures: The interatomic distances around 6 Å correspond to the separation between next-nearest neighbors within one hexagon. Due to the alternating Gd spin direction around this hexagonal motif, the correlation is always ferromagnetic for the concerned distances, which is not the case for $SrNd_2O_4$ as the magnetic structure is such that for a given Nd spin - roughly aligned along the b axis - one of the two next-nearest neighbors within one hexagon is predominantly antiparallel. The observed mPDF signal at that particular distance is not zero, because only one of the two Nd sites (Nd1 as defined in Fig. 1) carries a large ordered moment, and one can verify in Fig. 4(d) that all Nd1-Nd1 next-nearest-neighbors within a given hexagon have spins with antiparallel b components.

The limited beam time at D4, as well as the smaller available mass of the Nd compound and its smaller magnetic moment compared to Gd, all led to D4 data of relatively low

counting statistics as can be appreciated from the data-point scatter in Fig. 2(b). This Q-space noise leads to Fourier artifacts in real space with strong oscillations producing peaks at positions where no interatomic distance is present in the structure, as can be seen in the blue curves of Fig. 6(b). Quite remarkably the RMC fits in reciprocal space, since they result from real 3D spin-configurations, serve to "clean up" the Q-space data such that these Fourier artifacts are mostly eliminated, as can be seen in Fig. 6, where NN intra-chain AF correlations are still visible at 10 K for the Nd compound, and at 30 K for the Gd compound, for the dashed-green and dotted-red curves. Further evidence for the robustness of our results is given by the quantitative agreement between the D4 and D20 data for $SrNd_2O_4$ at 4.1 K in Q-space and in their spin-correlation functions.

IV. CONCLUSION

In this study we have illustrated the complementary utility of RMC simulations and mPDF-analysis for the treatment of magnetic diffuse scattering measured by total-scattering powder neutron diffraction. Whereas the spin-correlation functions derived from the RMC simulations provide reliable site-specific information about the relative alignment of two spins at a given distance r, the mPDF(r) as a direct Fourier transform of the total-scattering data has less resolution in r-space but retains information that determines whether the alignment of two spins is longitudinal or transverse in nature. The complementary use of both real-space methods provides a powerful tool for probing not only all static spin-correlations below T_N, but also *dynamic* short-ranged spin-correlations well above T_N, thus helping to understand the onset of magnetic ordering, especially in the case of frustrated magnetic systems.

Our data analysis clearly shows that nearest-neighbor and next-nearest-neighbor spins within a given zig-zag ladder are short-range dynamically correlated at a temperature of approximately 25 K and 15 K for $SrGd_2O_4$ and $SrNd_2O_4$, respectively, which corresponds to roughly 8 or 9 times T_N. By contrast, the short-range correlations between spins of neighboring zig-zag ladders become significant at only a few degrees above T_N. Our results confirm that the primary magnetic exchange interactions to consider are between spins of the same zig-zag ladder. The interactions at the slightly longer distances between spins of different zig-zag ladders play a secondary, but yet decisive role in the establishment of static long-range magnetic order. Finally, we observe in the Nd compound qualitatively different

spin correlations above T_N, as compared to those below T_N, between neighboring 1D chains, suggesting the formation of short-ranged dynamically-correlated, *i.e.* metastable, magnetic domains as T descends towards T_N, much before the static long-range order sets in below T_N. Based on the present data it is, however, not possible to extract a precise energy or length scale for these weak, metastable correlations which, obviously, should be comparable to the thermal energy kT. Further high-statistics or even single-crystal data might shed light into the highly interesting dynamical ordering in $SrLn_2O_4$ systems.

Acknowledgments

---

* Corresponding author. Electronic address: qureshi@ill.fr

[1] H. Karunadasa, Q. Huang, B. G. Ueland, J. W. Lynn, P. Schiffer, K. A. Regan, and R. J. Cava, Phys. Rev. B **71**, 144414 (2005).

[2] T. H. Cheffins, M. R. Lees, G. Balakrishnan, and O. A. Petrenko, J. Phys.: Condens. Matter **25**, 256001 (2013).

[3] A. Fennell, V. Y. Pomjakushin, A. Uldry, B. Delley, B. Prévost, A. Désilets-Benoit, A. D. Bianchi, R. I. Bewley, B. R. Hansen, T. Klimczuk, et al., Phys. Rev. B **89**, 224511 (2014).

[4] N. Gauthier, B. Prévost, A. Amato, C. Baines, V. Pomjakushin, A. D. Bianchi, R. J. Cava, and M. Kenzelmann, J. Phys.: Conf. Ser. **828**, 012014 (2017).

[5] N. Gauthier, A. Fennell, B. Prévost, A.-C. Uldry, B. Delley, R. Sibille, A. Désilets-Benoit, H. A. Dabkowska, G. J. Nilsen, L.-P. Regnault, et al., Phys. Rev. B **95**, 134430 (2017).

[6] O. Young, A. R. Wildes, P. Manuel, B. Ouladdiaf, D. D. Khalyavin, G. Balakrishnan, and O. A. Petrenko, Phys. Rev. B **88**, 024411 (2013).

[7] J.-J. Wen, W. Tian, V. O. Garlea, S. M. Koohpayeh, T. M. McQueen, H.-F. Li, J.-Q. Yan, J. A. Rodriguez-Rivera, D. Vaknin, and C. L. Broholm, Phys. Rev. B **91**, 054424 (2015).

[8] D. L. Quintero-Castro, B. Lake, M. Reehuis, A. Niazi, H. Ryll, A. T. M. N. Islam, T. Fennell, S. A. J. Kimber, B. Klemke, J. Ollivier, et al., Phys. Rev. B **86**, 064203 (2012).

[9] O. Young, G. Balakrishnan, M. R. Lees, and O. A. Petrenko, Phys. Rev. B **90**, 094421 (2014).

[10] N. Qureshi, B. Z. Malkin, S. X. M. Riberolles, C. Ritter, B. Ouladdiaf, G. Balakrishnan,

M. Ciomaga Hatnean, and O. A. Petrenko, Phys. Rev. B **105**, 014425 (2022).

[11] S. G. Tresvyatskii, V. N. Pavlikov, and L. M. Lopato, Inorg. Mater **6**, 33 (1970).

[12] W. Wong-Ng, Powder Diffr. **10**, 56 (1995).

[13] N. Qureshi, A. R. Wildes, C. Ritter, B. Fåk, S. X. M. Riberolles, M. Ciomaga Hatnean, and O. A. Petrenko, Phys. Rev. B **103**, 134433 (2021).

[14] N. Qureshi, J. Appl. Cryst. **52**, 175 (2019).

[15] B. Z. Malkin, S. I. Nikitin, I. E. Mumdzhi, D. G. Zverev, R. V. Yusupov, I. F. Gilmutdinov, R. Batulin, B. F. Gabbasov, A. G. Kiiamov, D. T. Adroja, et al., Phys. Rev. B **92**, 094415 (2015).

[16] O. A. Petrenko, G. Balakrishnan, N. R. Wilson, S. de Brion, E. Suard, and L. C. Chapon, Phys. Rev. B **78**, 184410 (2008).

[17] T. J. Hayes, G. Balakrishnan, P. P. Deen, P. Manuel, L. C. Chapon, and O. A. Petrenko, Phys. Rev. B **84**, 174435 (2011).

[18] N. Qureshi, O. Fabelo, P. Manuel, D. D. Khalyavin, E. Lhotel, S. X. M. Riberolles, G. Balakrishnan, and O. A. Petrenko, SciPost Phys. **11**, 007 (2021).

[19] J. A. M. Paddison, J. R. Stewart, and A. L. Goodwin, J. Phys.: Condens. Matter **25**, 454220 (2013).

[20] A. J. Freeman, and J. P. Desclaux, J. Mag. Magn. Mater. **12**, 11 (1079).

[21] B. A. Frandsen, X. Yang, and S. J. L. Billinge, Acta Crystallogr., Sect. A: Found. Crystallogr. **70**, 3 (2013).

[22] H. E. Fischer, G. J. Cuello, P. Palleau, D. Feltin, A. C. Barnes, Y. S. Badyal, and J. M. Simonson, Appl. Phys. A **74**, S160 (2002).

[23] S. Riberolles, H. E. Fischer, and N. Qureshi, Institut Laue-Langevin (ILL) doi:10.5291/ILL-DATA.INTER-355 (2017).

[24] M. A. Howe, R. L. McGreevy, and P. Zetterstrom, NFL Studsvik internal report (1996).

[25] T. C. Hansen, P. F. Henry, H. E. Fischer, J. Torregrossa, and P. Convert, Meas. Sci. Technol. **19**, 034001 (2008).

[26] H. E. Fischer, T. Hansen, and N. Qureshi, Institut Laue-Langevin (ILL) doi:10.5291/ILL-DATA.TEST-3061 (2019).

[27] Yu. I. Dublenych, and O. A. Petrenko, SciPost. Phys. Core **5**, 47 (2022).

Figures

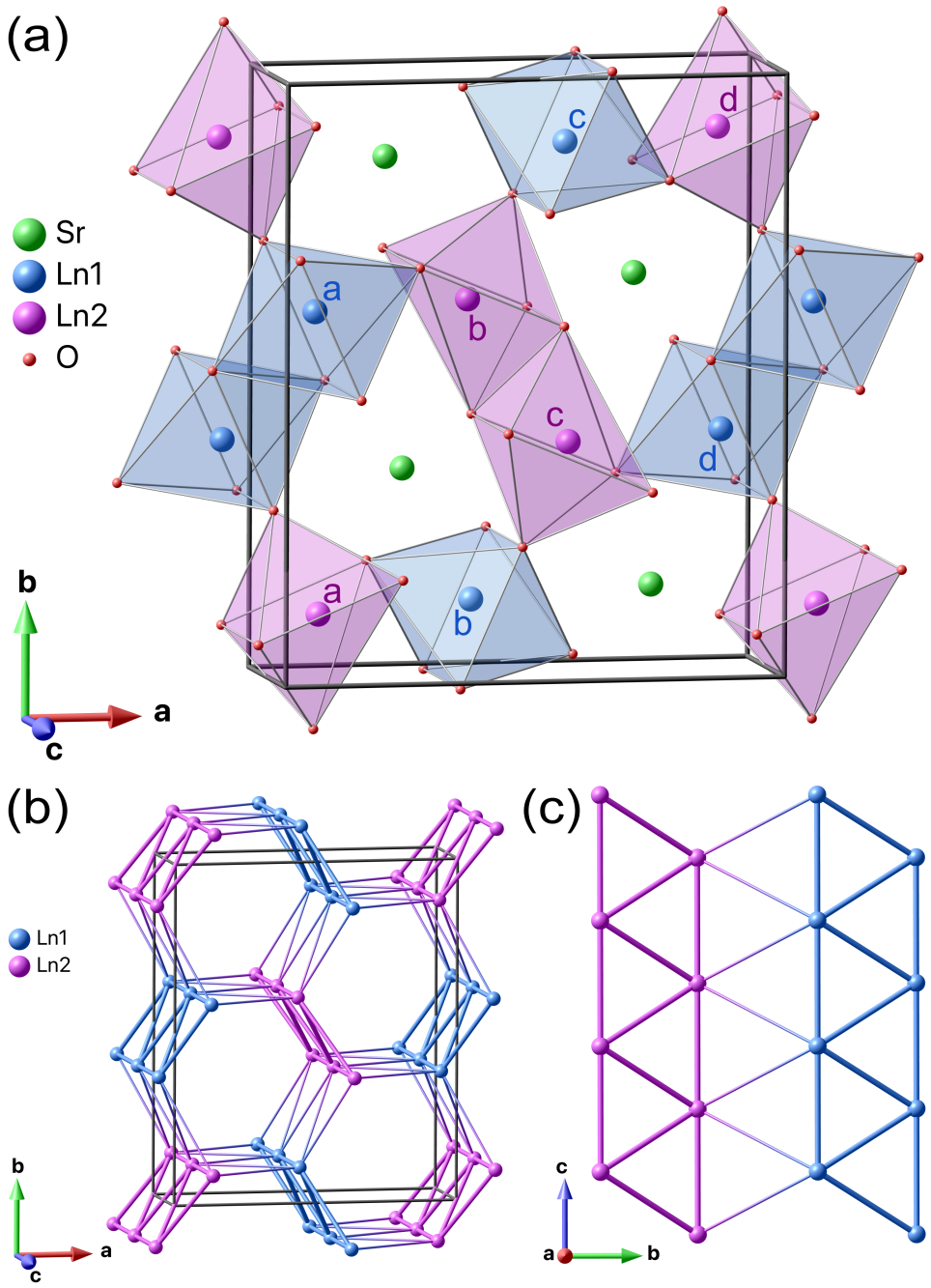

FIG. 1: (a) Perspective view of the unit cell of the $SrLn_2O_4$ compound. The magnetic Ln ions on the two distinct 4*c* sites are shown by large spheres (blue and violet; oxygen and Ln ions are shown in red and green, respectively) and are labeled from *a* to *d* with increasing *x* component. (b) Visualization of the distorted honeycomb structure (only showing the magnetic ions) in the *ab*-plane forming zig-zag ladders of two types running along the *c* direction as shown in (c). The figures were created using the MAG2POL programme.[14]

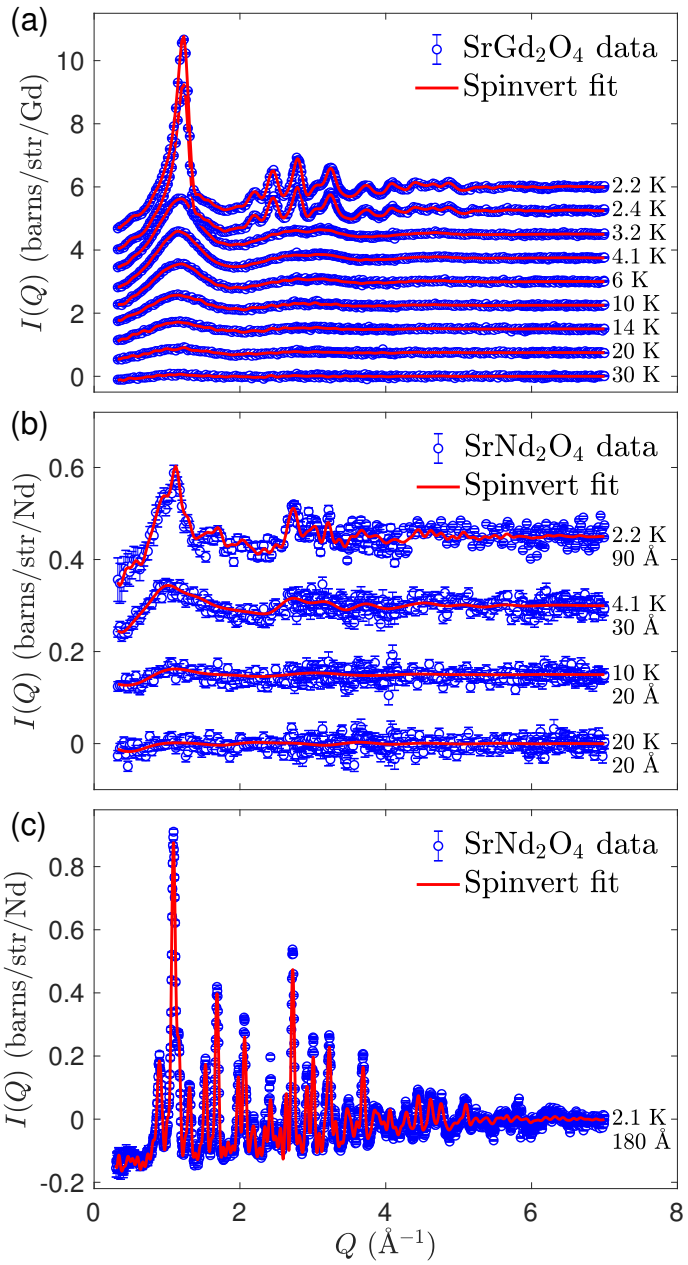

FIG. 2: Magnetic scattered intensity [open (blue) circles] - obtained by subtracting a paramagnetic baseline pattern at 50 K - in absolute units at different temperatures as a function of scattering vector Q for (a) $SrGd_2O_4$ (D4, 90 Å box), (b) $SrNd_2O_4$ (D4, box size is shown below the temperature label) and (c) for $SrNd_2O_4$ as obtained on the D20 diffractometer within the long-range ordered magnetic phase at $T = 2.1$ K using a simulation box of 180 Å. The (red) solid lines are the result of the RMC simulations described in the text. For clarity the curves in (a) and (b) have been shifted vertically by 0.75 barns/str/Gd-atom and 0.15 barns/str/Nd-atom, respectively.

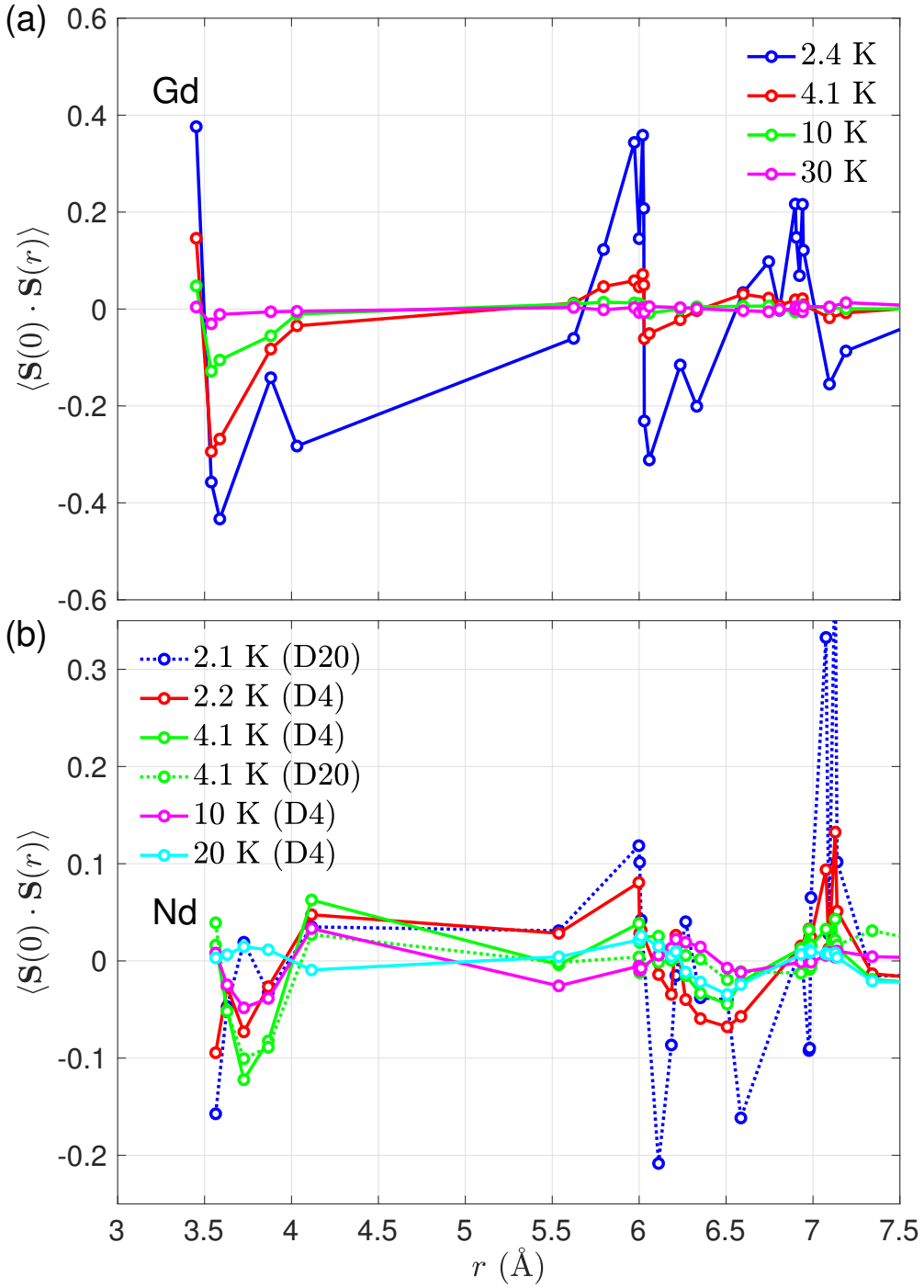

FIG. 3: Spin-correlation function (SCF) $\langle \mathbf{S}(0) \cdot \mathbf{S}(r) \rangle$ for interatomic distances up to 7.5 Å in (a) $SrGd_2O_4$ and (b) $SrNd_2O_4$ at selected temperatures. Non-zero short-range correlations are clearly observable well above T_N. The significant correlations at larger distances are indicative of the onset of long-range magnetic order.

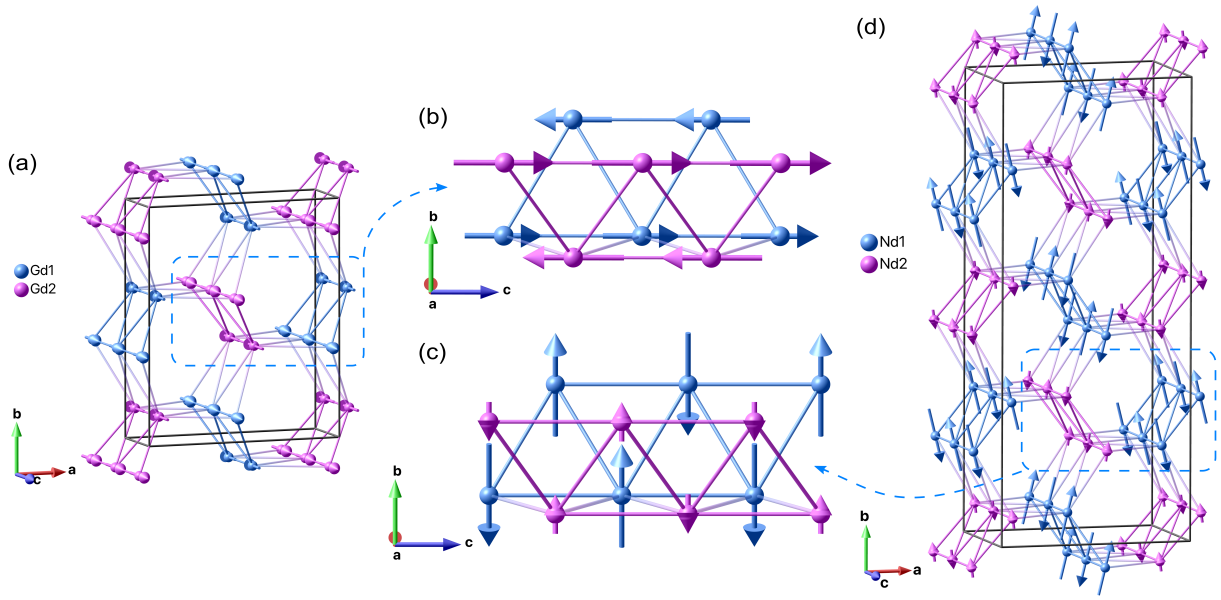

FIG. 4: (a) Perspective view of the magnetic structure in the intermediate temperature phase in $SrGd_2O_4$ revealing a longitudinal spin alignment along the one-dimensional chains along the b axis with differently sized ordered moments for the two Gd sites. Nearest-neighbors are indicated by opaque unicolor bonds, while inter-ladder connections are shown by semi-transparent bicolor bonds. Two antiferromagnetically aligned 1D chains composed of the same site form J_1-J_2 zig-zag ladders where the next-nearest neighbor interactions are represented in blue and purple. The dashed rectangle shows the part of the zig-zag ladder that (b) focuses on. (c) Perspective view of the magnetic structure in $SrNd_2O_4$ showing a transversal spin alignment with respect to the chain direction with different ordered moment sizes for the two Nd sites. The zig-zag ladder marked by the dashed rectangle is enlarged in (d). The figures were created using the MAG2POL programme.[14]

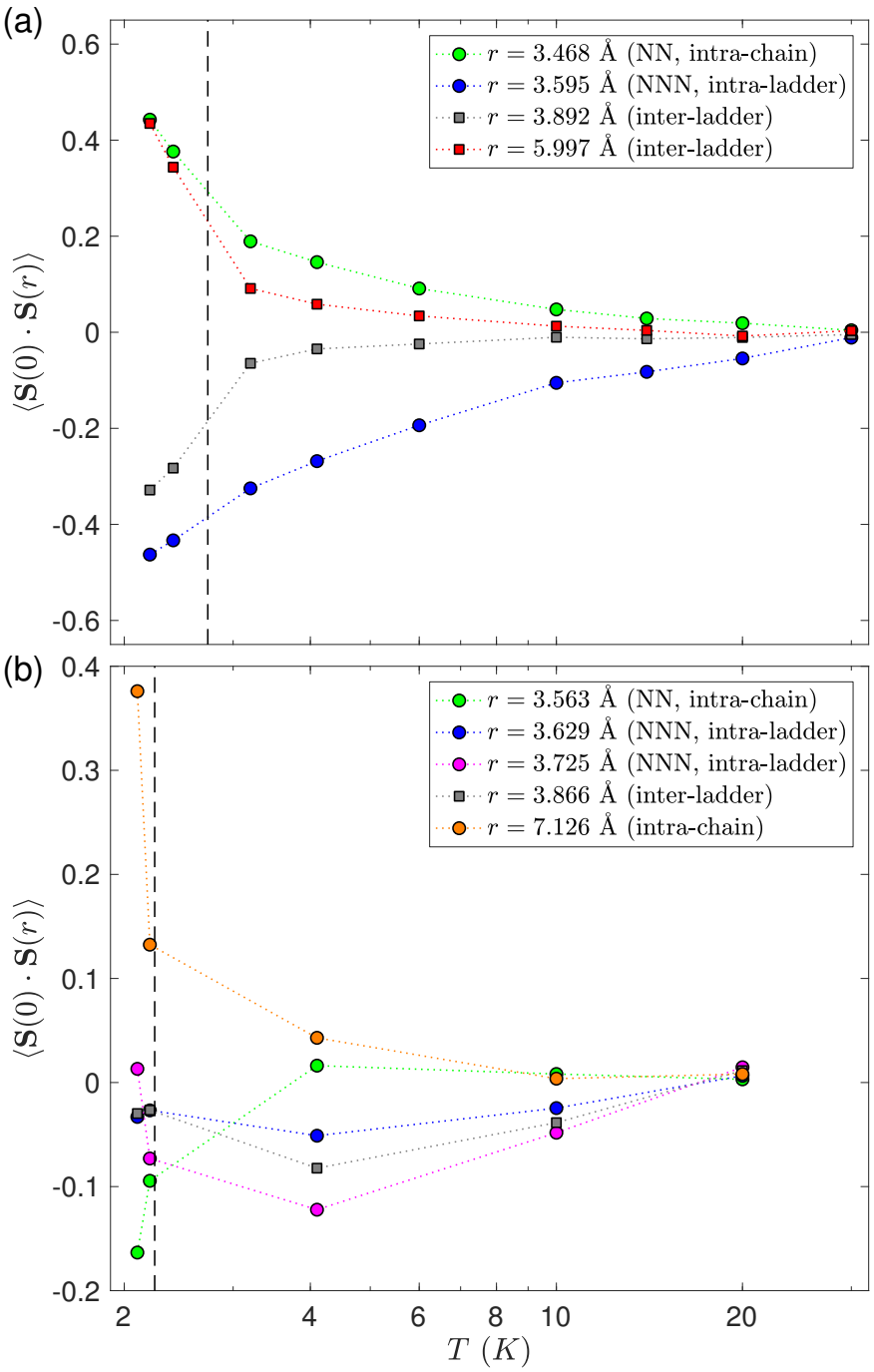

FIG. 5: Spin-correlation function (SCF) $\langle \mathbf{S}(0) \cdot \mathbf{S}(r) \rangle$ for selected intra- and inter-zig-zag ladder distances in (a) $SrGd_2O_4$ and (b) $SrNd_2O_4$. Significant intra-chain correlations (circles) are observed far above the Néel temperature (marked by a vertical dashed line). Inter-ladder correlations (squares) become important at only a few K above T_N.

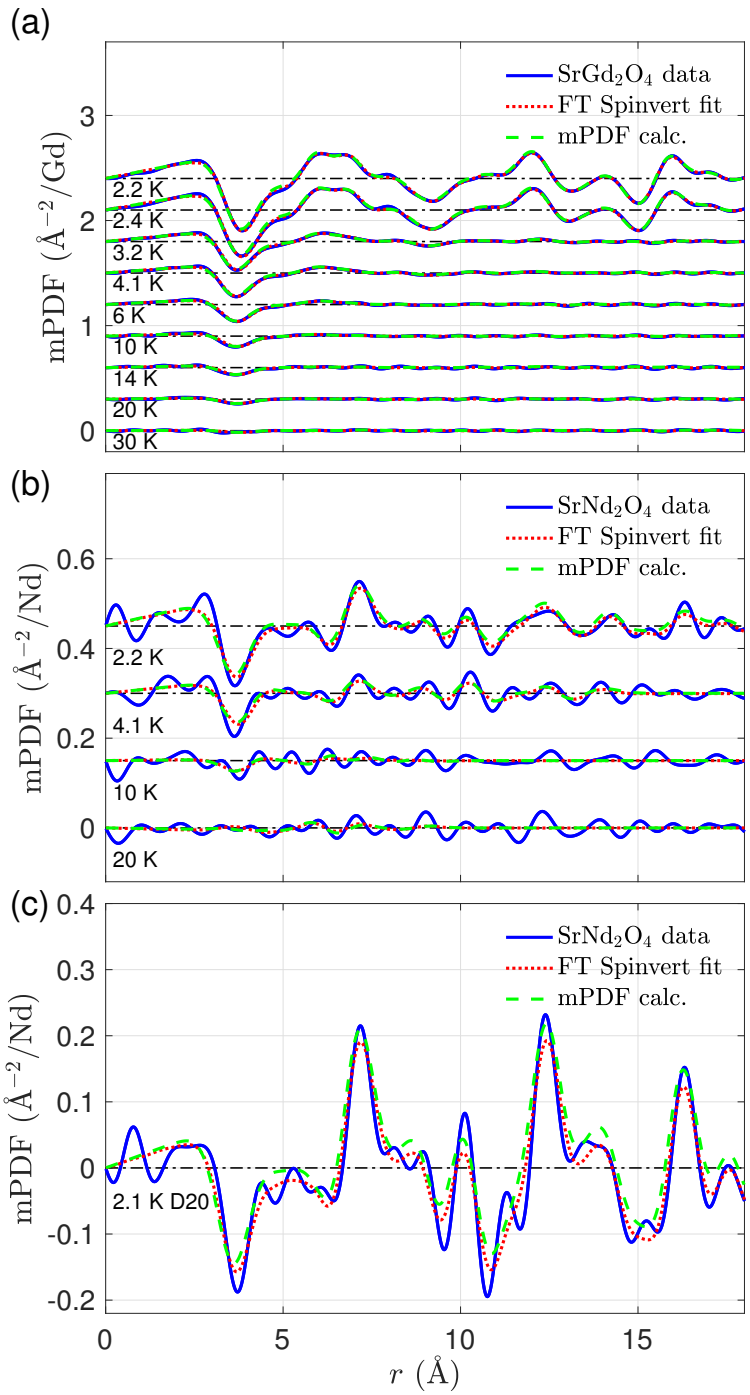

FIG. 6: Magnetic pair distribution function mPDF(r) shown for interatomic distances $r < 18$ Å in (a) $SrGd_2O_4$, (b) $SrNd_2O_4$ above T_N (D4) and (c) below T_N (D20). Solid (blue) lines show the respective corrected data, dotted (red) lines represent the Fourier transformed RMC fit and dashed (green) lines stand for the calculated mPDF profiles according to the RMC results and Eq. 2. The curves are shifted vertically by 0.3 and 0.15 Å^{-2}/Ln for clarity in (a) and (b), respectively. The dash-dotted lines are the zero-lines of the corresponding mPDF.

Tables

TABLE I: Interatomic Ln-Ln distances r up to 7.5 Å for $SrGd_2O_4$ and $SrNd_2O_4$ (at $T = 4$ K and 5 K, respectively, based on the structural data in Refs. 10,13) as shown in Fig. 3 with the corresponding atom pairs. The labeling is according to Fig. 1(a) with 1 and 2 referring to the different Ln sites and *a*-*d* denoting the different positions. A lattice vector $[uvw]$ is added to the second atom of a pair, if it is located in a different unit cell. Note that the distances $r_{Gd} = 3.468$ Å ($r_{Nd} = 3.564$ Å) and $r_{Gd} = 6.936$ Å ($r_{Nd} = 7.128$ Å) correspond to once or twice the lattice constant c in the Gd (Nd) compound.

r_{Gd} (Å)	r_{Nd} (Å)	Atom 1 − Atom 2	r_{Gd} (Å)	r_{Nd} (Å)	Atom 1 − Atom 2
3.468	3.564	$1a - 1a + [001]$	6.261	6.353	$1a - 2b + [002]$
3.563	3.630	$1a - 1d + [\bar{1}00]$	6.361	6.507	$1a - 2d + [\bar{1}02]$
3.595	3.726	$2b - 2c$	6.641	6.585	$1a - 2c + [\bar{1}01]$
3.892	3.867	$1a - 2b$	6.757	6.977	$1a - 2c + [001]$
4.051	4.115	$1a - 2d + [\bar{1}00]$	6.839	6.931	$1a - 2b + [\bar{1}00]$
5.664	5.537	$1a - 2c + [\bar{1}00]$	6.928	6.981	$1a - 2a + [011]$
5.799	5.998	$1a - 2c$	6.936	7.128	$1a - 1a + [002]$
5.997	6.003	$1a - 2a + [010]$	6.952	6.988	$1a - 1c + [001]$
6.025	6.011	$1a - 1c$	6.968	7.139	$1a - 2a + [001]$
6.043	6.185	$1a - 2a$	6.974	7.075	$2a - 2c + [001]$
6.050	6.112	$2a - 2c$	7.131	7.091	$2a - 2b$
6.062	6.211	$1a - 1d + [\bar{1}02]$	7.206	7.340	$1a - 1b$
6.081	6.268	$2a - 2d + [\bar{1}\bar{1}2]$			